Tellus (2007), 59B, 425–438
Printed in Singapore. All rights reserved

TELLUS

The surface energy, water, carbon flux and their intercorrelated seasonality in a global climate-vegetation coupled model

By LI DAN* and JINJUN JI, *START Regional Center for Temperate East Asia and Key Laboratory of Regional Climate-Environment for Temperate East Asia, Institute of Atmospheric Physics, Chinese Academy of Sciences, Beijing, 100029*

(Manuscript received 29 April 2006; in final form 24 January 2007)

ABSTRACT

The sensible and latent heat fluxes, representatives of the physical exchange processes of energy and water between land and air, are the two crucial variables controlling the surface energy partitioning related to temperature and humidity. The net primary production (NPP), the major carbon flux exchange between vegetation and atmosphere, is of great importance for the terrestrial ecosystem carbon cycle. The fluxes are simulated by a two-way coupled model, Atmosphere-Vegetation Interaction Model-Global Ocean-Atmosphere-Land System Model (AVIM-GOALS) in which the surface physical and physiological processes are coupled with general circulation model (GCM), and the global spatial and temporal variation of the fluxes is studied. The simulated terrestrial surface physical fluxes are consistent with the 40-yr European Centre for Medium-Range Weather Forecasts (ECMWF) Reanalysis (ERA40) in the global distribution, but the magnitudes are generally 20–40 W/m^2 underestimated. The annual NPP agrees well with the International Geosphere Biosphere Programme (IGBP) NPP data except for the lower value in northern high latitudes. The surface physical fluxes, leaf area index (LAI) and NPP of the global mid-latitudes, especially between 30 °N–50 °N, show great variation in annual oscillation amplitudes. And all physical and biological fields in northern mid-latitudes have the largest seasonality with a high statistical significance of 99.9%. The seasonality of surface physical fluxes, LAI and NPP are highly correlated with each other. The meridional three-peak pattern of seasonal change emerges in northern mid-latitudes, which indicates the interaction of topographical gradient variation of surface fluxes and vegetation phenology on these three latitudinal belts.

1. Introduction

The exchange of mass, energy and momentum between the land and atmosphere is of great importance for climate studies, thus it is parametrized in many land surface models (LSMs) with different schemes (Pitman et al., 1999). The surface sensible heat flux (SH) and the latent heat flux (LH) are the key variables that control the energy partitioning related to the phase change of water and the temperature gradient change between land and air (Varejao-Silva et al., 1998; Chen and Dudhia, 2001). The variation of SH and LH can affect climate through a strong impact on the evolution of atmospheric boundary layer (Koster et al., 2002), e.g. the strong cooling effect of evapotranspiration (ET) on surface temperature and the conductive-convective transfer of sensible heat to the atmospheric boundary layer from land surface (Shukla and Mintz, 1982). The net primary production (NPP), a crucial component for the terrestrial carbon cycle, is the net accumulation of photosynthetically fixed carbon from vegetation utilizing the sunlight, water and carbon dioxide to produce carbohydrate. The photosynthesis and vegetation respiration are related to the canopy temperature, which is closely related to the air temperature and soil temperature change through land-air energy and water exchange. In seasonal environment, presence or absence of leaves will not only affect surface energy partitioning (since ET in leaf-less ecosystems will be greatly reduced) but also the aerodynamic resistance of the surface and the surface-atmosphere exchange of momentum. There have been some studies (Cox et al., 2000; Friedlingstein et al., 2001) using coupled models to show that the future global warming will be enhanced by including positive feedback effects from the terrestrial carbon cycle. Consequently, the surface physical fluxes and carbon flux (NPP for this study) should be coupled tightly in order to study their interaction as suggested by the previous work (Ji, 1995; Sellers et al., 1997).

Validation of some components of coupled climate-vegetation models can be attempted, for instance, with regionally or

*Corresponding author.
e-mail: danli@tea.ac.cn
DOI: 10.1111/j.1600-0889.2007.00274.x

globally integrated NPP products that are based on a combination of ground-based and satellite remote sensing observations (Zheng et al., 2003). Naturally, similar to the general circulation model (GCM) output, these data-based products have also uncertainties associated with them, either because they are based on upscaled surface information that is only available for some regions (e.g. China, USA, Australia; Zheng et al., 2003), or because they are based on terrestrial carbon cycle models driven by remotely sensed vegetation cover (Imhoff et al., 2004; Cao et al., 2005). Uncertainties are possibly smaller for benchmarking data sets of the energy fluxes at regional or global scale, since the reanalysis data available from the European Centre for Medium-Range Weather forecast (ECMWF) (Simmons and Gibson, 2000) can be used as the comparison data for surface physical fluxes (SPFs).

Despite facilitation of the reanalysis data, the SPFs simulated by GCMs and regional climate models (RCMs) still show a large discrepancy due to the different parametrization schemes and other mechanism uncertainties of these models. The Project for Intercomparison of Land-surface Parametrization Schemes (PILPS) numerical experiments (Shao and Henderson-Sellers, 1996; Chen et al., 1997; Pitman, et al., 1999) show that despite being driven by the same forcing conditions, the simulated SPFs, soil moisture, and runoff of different LSMs varied considerably. However, these discrepancies may help modellers to better understand the limitations of individual models (Chen and Dudhia, 2001). Compared to the largely successful simulation of global climate of air temperature and precipitation (Xue et al., 2004; Dan et al., 2005), the modelled SPFs need further study such as the quantitative intercomparison of the physical flux simulation to the reanalysis data. The intercomparison will be helpful to comprehend the uncertainty of SPFs and improve the capacity of LSMs in capturing nature of the spatial and temporal variation of land/air exchange processes.

In this study, the surface energy flux, water flux and terrestrial carbon cycle were linked together in the global two-way coupled model AVIM-GOALS. The two-way coupling initiates the dynamical vegetation processes into GCMs and overcomes the deficiency of prescribed vegetation parameters (e.g. LAI) of LSMs in climate models (Dan et al., 2005). This kind of interactive physical and biological model provides a useful tool to study the SPFs and carbon flux within a single climate model framework. Also explored was the spatiotemporal variation of the SPFs, LAI and NPP as well as their interrelation in the seasonal cycle. From the perspective of global mean scale, the principal regional contribution to the seasonal fluctuation of the SPFs, LAI and NPP was analyzed.

2. Model and data descriptions

2.1. Model (LSM and GCM) descriptions

The land surface model used here is Atmosphere-Vegetation Interaction Model (AVIM), which is a LSM incorporating the physical processes (Ji and Hu, 1989) and eco-physiological processes (Ji, 1995). This model has one canopy layer and ten uneven soil layers, and the physical and chemical boundary conditions in the deepest soil layer are assumed constants. Sensible and latent heat fluxes from the ground and the canopy are calculated by the method in the electric analogue form, which considers a flux as proportional to the ratio between a potential difference and a resistance. The energy, momentum and water exchange between land and air are linked with vegetation growth processes and terrestrial ecosystem carbon cycles through physiological activities of photosynthesis, respiration and morphological change (Dan et al., 2005). The vegetation morphology is affected by the accumulation, consumption and allocation of dry matter. Surface characteristic parameters, such as albedo, dynamical roughness length, zero plane displacement and resistance parameters including the stomata resistance are affected by the vegetation morphological parameters, e.g. LAI and root density.

The SPFs, a boundary condition for the GCM, are parametrized as:

$$\mathrm{H} = \rho\delta C_{\mathrm{p}}(\theta_{\mathrm{ac}} - \theta_{\mathrm{a}})/r_{\mathrm{a}} \tag{1}$$

$$\mathrm{E_L} = L\rho(q_{ac} - q_a)/r_a \tag{2}$$

Where H, $\mathrm{E_L}$ are the sensible heat and water vapour fluxes between the air and land, and ρ, C_{p} are surface air density and specific heat at constant pressure. δ is a factor related to the sigma coordinate of the GCM. θ_{ac}, $q_{\mathrm{ac},}$ r_{a} are air potential temperature, specific humidity and aerodynamical resistance within the canopy, respectively (see the appendix A2–A3 of Lu and Ji, 2006). θ_{a}, q_{a} are potential temperature and specific humidity at the bottom layer of the GCM. L is the latent heat of evaporation.

The NPP equation is expressed as follows:

$$NPP = GPP - R_{\mathrm{m}} - R_{\mathrm{g}} \tag{3}$$

Where GPP is the gross photosynthesis rate excluding photorespiration, R_{m} is the maintenance respiration rate, and R_{g} is the growth respiration rate. Here, the photosynthesis adopts an improved scheme based on the biochemistry (Lu and Ji, 2002a) compared to the Michaelis-MentEn form in the previous version of AVIM (Ji, 1995), and the details of this new scheme of photosynthesis are presented by Lu and Ji (2006). The gross photosynthesis rate is upscaled from leaf to canopy as follows

$$GPP = \int_0^{\mathrm{LAI}} A(L)\,dL = \int_0^{\mathrm{LAI}} A_0 e^{-KL} dL = \frac{1 - e^{-K\cdot\mathrm{LAI}}}{K} A_0 \tag{4}$$

A_0 is photosynthesis rate at the top of canopy and K is the extinction coefficient of photosynthetically active radiation (PAR). LAI is a key parameter for the feedback between physical-physiological processes (Lu and Ji, 2006) and can be calculated by

$$\mathrm{LAI} = M_f SLA \tag{5}$$

Where M_f is the foliage biomass and SLA is the specific leaf area (Schulze et al., 1994), based on the previous work (Farquhar et al., 1980; Collatz et al., 1992; and Woodward et al., 1995):

$$A_0 = \min(w_c, w_j) \tag{6}$$

w_c is Rubisco limited carboxylation rate, w_j is the RuBP limited rate of carboxylation in the Calvin cycle. Rubisco, ribulose-1,5-bisphosphate carboxylase, is an enzyme as the catalyst in the photosynthesis to create organic carbon from the inorganic carbon dioxide in the air. Rubisco takes carbon dioxide and attaches it to ribulose-1,5-bisphosphate (RuBP), a short sugar chain with five carbon atoms.

$$w_c = V_{c\max} \frac{C_i - \Gamma^*}{C_i + K_c(1 + O_i/K_o)} \tag{7}$$

Where $V_{c\max}$ is the maximum carboxylation rate at saturation of RuBP and oxygen, C_i is the CO_2 concentration in leaf interior, Γ^* is the compensation point in the absence of photorespiration, O_i is the oxygen concentration in leaf interior, K_c and K_o are the Michaelis-MentEn constants for CO_2 and O_2.

$$V_{c\max} = V_{c\max 25} f(N) f(W_s) f(T) \tag{8a}$$

$$f(T) = Q_{10}^{0.1(T-T_0)} \tag{8b}$$

$$f(W_s) = (1 - e^{-b|w-w_i|})^{-1} \tag{8c}$$

$$f(N) = 1 \tag{8d}$$

Where $V_{c\max 25}$ is the value of $V_{c\max}$ at 25 °C, $f(N)$, $f(W_s)$ and $f(T)$ are effects of leaf nitrogen concentration (Field, 1983), soil moisture and canopy temperature on $V_{c\max}$, respectively. Q_{10} is the temperature coefficient with the value of 2.0, T_0 is a reference temperature, T is the canopy temperature, b is a constant, w is the soil moisture of the first layer and w_i is the corresponding wilting point of soil moisture. In this study, the effect of leaf nitrogen concentration is not considered and we assume $f(N)=1$.

$$w_j = \frac{J}{4} \frac{C_i - \Gamma^*}{C_i + \Gamma^*} \tag{9}$$

The calculation of C_i is supposed to be a function of the specific humidity deficit of the canopy (Jacobs et al., 1996) and has been given by Lu and Ji (2006).

$$f \equiv \frac{C_i - \Gamma^*}{C_s - \Gamma^*} = f_0\left(1 - \frac{D_s}{D_{s\max}}\right), \tag{10}$$

Where $D_s = q_s(T) - q_{ac}$ is the leaf-to-air specific humidity deficit and is similar to the vapor pressure deficit (VPD), C_s is the CO_2 concentration at the leaf surface, f_0 is the value of f at $D_s = 0$ and $D_{s\max}$ is the maximum value of D_s when the stomata are closed.

The canopy conductance g_s is linked with photosynthesis by the following equation: $g_s = \frac{1.6A_c}{C_s - C_i}$ (Farquhar et al., 1980; Farquhar and Sharley, 1982; Jacobs et al., 1996), where $A_C =$ GPP, and we get

$$g_s = \frac{1}{r_f} = \frac{1.6A_c}{(C_s - \Gamma^*)(1 - f)}, \tag{11}$$

Where r_f is the canopy resistance, which affects CO_2 and H_2O vapour diffusion in and out of the leaf.

J is the light-saturated rate of electron transport

$$J = \alpha Q = 4.6\alpha \mathrm{PAR}, \tag{12}$$

Where α is quantum yield of electron transport and Q is the absorbed quantum flux(μ mol photon $m^{-2}s^{-1}$).

$$R_{mi} = \alpha_i M_i \times Q_{10}^{0.1\cdot(T-T_0)} \quad i = f, s, r \tag{13}$$

Here, M_i is biomass of each tissue and the subscripts *f, s, r* represent leaves, stems and roots, respectively. α_i is a constant coefficient, T is the canopy temperature for leaf and stem and the soil temperature for root (Ji et al., 2005), R_m is the sum of maintenance respiration of the three vegetation components (Lu and Ji, 2006).

$$R_{gi} = \eta_i \frac{dM_i}{dt} \quad i = f, s, r \tag{14}$$

Where η_i is the allocation coefficients for the leaves, stems and roots with $\sum_i \eta_i = 1$, dM_i/dt is the growth rate for the three components (Li and Ji, 2001, Ji et al., 2005), and $R_{gi} = 0$ if $dM_i/dt \le 0$. Total growth respiration is equal to sum of the three components. The phenological phase is assumed to be controlled by the growing-degree days temperature sum (above 5 °C), and the falling leaves are dependent on the life time of the leave, which is similar to the phenology used by Lu and Ji (2006).

The principal input variables from the climate model are shown in Table 1. They include nine basic variables from atmospheric boundary layer: air temperature, specific humidity, precipitation, two components of wind speed, surface air pressure, surface downward short- and long-wave radiation, and atmospheric CO_2 pressure. The principal prognostic variables are presented in Table 2. They include seven surface physical fields

Table 1. The principle input variables used in AVIM from the GCM

Symbol	Definition	Unit
T	Air temperature	K
q	Air specific humidity	$kgkg^{-1}$
Prp	Precipitation/snow	ms^{-1}
U	Zonal wind speed	ms^{-1}
V	Meridional wind speed	ms^{-1}
Pre	Atmospheric surface pressure	Pa
S_W	Atmospheric surface short wave radiation	Wm^{-2}
L_W	Atmospheric surface long wave radiation	Wm^{-2}
CO_2	Atmospheric CO_2 pressure	Pa

Table 2. The principle outputs or prognostic variables of the two-way coupled model over land

Symbol	Definition	Unit
S_H	Surface sensible heat flux	Wm^{-2}
L_H	Surface latent heat flux	Wm^{-2}
T_i	Soil temperature of each layer	K
M_c	Water stored in the canopy	m
W_i	Soil moisture of each layer	m^3m^{-3}
α_f	Albedo of vegetation	fraction
S_g	Snow depth at land surface	m
LAI	Leaf area index	m^2m^{-2}
NPP	Net primary production	gCm^{-2}
BM_i	Biomass of leaf, stem and root.	gCm^{-2}

of energy and water budget, and three variables related to vegetation morphology and dry matter accumulation.

AVIM has been validated in many basic ecosystems including forests, grasslands, shrublands and croplands (Ji and Yu, 1999; Li and Ji, 2001; Lu and Ji, 2002b; Dan et al., 2005). The simulations reveal the reasonable spatiotemporal variation of NPP in relation to the climatic change in terms of air temperature and precipitation. AVIM has participated in the Ecosystem Model-Data Intercomparison (EMDI) organized by IGBP project on Global Analysis, Interpretation and Modelling (GAIM), and the simulated NPP agrees well with the measured NPP (Dan et al., 2005). The global soil texture data were taken from Zobler (1986) with six classification types. The plant function type is classified into 13 types similar to Xue et al. (2004).

The GCM, Global Ocean-Atmosphere-Land System Model (GOALS), is developed at Institute of Atmospheric Physics/State Key Laboratory of Numerical Modelling for Atmospheric Sciences and Geophysical Fluid Dynamics (IAP/LASG). This climate model has nine layers in the atmosphere and is truncated rhombically at the 15 wave numbers (Wu et al., 1997). The horizontal resolution is 7.5 ° longitude by 4.5 ° latitude. The reduction of a standard atmosphere proposed by Zeng (1963) and Phillips (1973) was used in the dynamical framework to improve the GCM performance. A new k-distribution radiation scheme (Wang et al., 2000) was introduced to make the cloud radiation processes more reasonable. The monthly mean climatologically observed sea surface temperature (SST) and sea ice was taken from the 1979–1988 data of Atmospheric Model Intercomparison Project (AMIP). The integration time step is 30 min and the land-air coupling is synchronous. The GOALS GCM performs well in global climate simulations, especially for the large-scale features and seasonal cycle (Liu et al., 2001). It has been used to study the climate changes, such as the maintenance mechanism of subtropical anticyclone (Liu et al., 2004) and future climate projection under different scenarios (Coquard et al., 2004).

Considering the coarse resolution of GOALS, the land surface model AVIM is designed to relatively fine grid of 1.5 ° by 1.5 ° and the interface coupling adopts the nesting technique to link the two models. Thus a unit grid of the GCM is subdivided into 15 grid cells down to the surface. The two-way coupled model has run for 30 yr, and the last 15 yr outputs were selected for the analysis.

2.2. *The ERA40 flux data, observation LAI and IGBP NPP data*

The sensible and latent heat flux reanalysis data in this study were provided by the European Centre for Medium-Range Weather Forecasts (ECMWF). The ECMWF 40-yr reanalysis (Simmons and Gibson, 2000) for surface physical fluxes (abbreviated as ERA40 flux data) was monthly daily mean fields with a resolution of 2.5 ° by 2.5 °. The observation LAI data provided by the Max Planck Institute for Meteorology were derived from the minimum and maximum values for fractional vegetation cover and LAI from the land surface parameters (LSP) dataset, monthly values for fraction of absorbed photosynthetically active radiation (FPAR), and a monthly 2 m temperature climatology in high latitudes (Hagemann et al., 1999; Hagemann, 2002). This dataset is 0.5 ° by 0.5 ° and it covers the global land areas excluding Greenland and Antarctica. The LSP dataset has been successfully used in the RCMs of HIRHAM and REMO as well as in the global European Centre Hamburg Model (ECHAM) model (Hagemann, 2002). The International Geosphere Biosphere Programme (IGBP) Global NPP Model Intercomparison Data (IGBP NPP data) with the resolution of 0.5 ° by 0.5 °, were downloaded from the website of International Satellite Land Surface Climatology Project Initiative II (ISLSCP II). The annual mean IGBP NPP data used to intercompare the simulated NPP of the coupled model AVIM-GOALS were derived from the original data containing gridded average NPP for 17 global models of biogeochemistry (Cramer et al., 1999).

3. Results and analysis

3.1. *The global SPFs, NPP and LAI*

(1) The SPFs simulations

The global distribution of SH and LH is shown in Fig. 1. The climatologically annual mean SH and LH is generally consistent with the ERA40 flux data. The maximum SH (greater than 60 W/m^2) is located in the arid or semi-arid regions of southern and eastern coast of Africa, Western China, Australia, and the West Coast of North and South America. The SH in tropical rainforests and boreal forests is below 20 Wm^{-2}, and the negative SH occurs in northern high latitudes. But the simulated SH in high latitudes is underestimated with the minimum of –40 Wm^{-2} compared to the –20 Wm^{-2} of ERA40 SH; the reason for this is the less net surface radiation (Zhang et al., 2002). The maximum SH simulation in Southern Africa and Australia is 40 Wm^{-2} lower than the ERA40 SH and this reflects the large discrepancies of SPFs

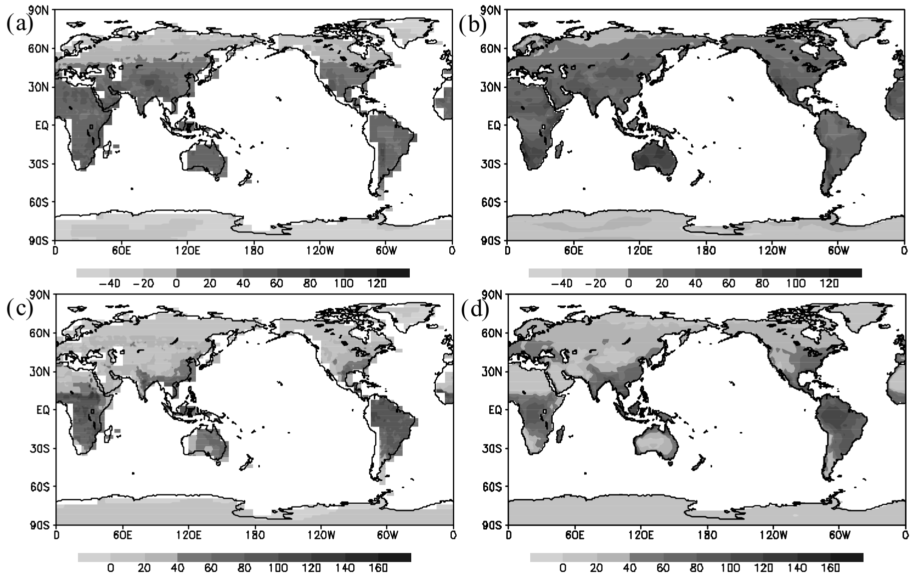

Fig. 1. Annual mean surface sensible heat flux (SH) and latent heat flux (LH) for the coupled model AVIM-GOALS and ERA40 reanalysis: (a) AVIM-GOALS SH, (b) ERA40 SH; (c) AVIM-GOALS LH, (d) ERA40 LH, units: Wm^{-2}.

simulation. The discrepancy can be easily understood according to the PILPS LSMs intercomparison result (Pitman, et al., 1999), which presents 79 Wm^{-2} range for SH and 80 W/m^2 for LH in annual mean simulations of tropical rainforests for different LSMs, and shows 34 and 27 Wm^{-2} range for SH and LH of grassland. The large SH centre in the Tibetan Plateau seems to be reasonable compared to the high value of the previous work (Gao and Lu, 1981; Lu and Ji, 2002a) in this region. The large LH occurs in the tropical rainforests (80–120 Wm^{-2}), followed by 40–80 W/m^2 in the temperate forests of southeast China and southeast USA, and 20–40 Wm^{-2} in boreal forests. Compared to the previous version of overestimated ERA15 LH data in southeast China (Figure not shown), the ERA40 LH shows the improvement with the July maximum slightly larger than the 100 Wm^{-2} according to the Climatological Atlas of China (Gao and Lu, 1981), whereas ERA15 July maximum LH presents large-area of 120 Wm^{-2} in this region.

The seasonal cycle of the exchanges of energy, mass and momentum between the land and atmosphere can be modified by vegetation through morphological change and carbon assimilation, and it plays a major role in the seasonal variations of local surface hydrology (Varejao-Silva et al., 1998). It is important to evaluate the seasonality of the coupled model to understand the capacity of simulating the seasonal change of SPFs and vegetation. Here, the seasonal variation range or oscillation amplitude for SH, LH, LAI and NPP was analyzed using the difference between boreal summer and winter values (representative of July minus January averages). Fig. 2 shows the seasonal oscillation amplitude of SH and LH. The simulated SH difference (Fig. 2a) agrees well with the ERA40 SH difference in that the positive SH difference above 40 Wm^{-2} is distributed to north of 30 °N. The large positive SH difference up to 80 Wm^{-2} emerges in the northern mid-latitudes (30–50 °N). The region centred about 15 °S of Africa and South America shows also the 0–40 W/m^2 positive difference. The noticeable negative SH difference below –40 Wm^{-2} occurs in the southern end of Africa, Australia and South America. The LH difference (Fig. 2c and d) exhibits a large winter-to-summer increase in northern mid-latitudes, but the simulation is about 20 Wm^{-2} lower than ERA40 LH variation that has maximum up to 100 Wm^{-2}. Unlike the SH difference pattern, the LH difference in Southern Hemisphere is nearly negative.

(2) The NPP simulations

Global human consumption proportion of terrestrial NPP is about 20% (range of 14–26%) of the total NPP generated on land (Imhoff et al., 2004). Due to the importance in human needs and climate change, many terrestrial ecosystem models attempted to simulate the global NPP patterns e.g. the IGBP NPP intercomparison work. The IGBP NPP data are considered to be a comprehensive representation of NPP fluxes (Cramer et al., 1999), so the simulated NPP of the coupled model was compared with the data. Fig. 3a is the multi-year annual mean NPP of the coupled model AVIM-GOALS, and the simulation is consistent with the IGBP NPP data (Fig. 3b). The largest annual NPP across the globe (with the value greater than 1000 $gCm^{-2}year^{1}$) is distributed through the tropical rainforests of Africa, Southeast Asia and Amozonia. The areas with 500–700 $gCm^{-2}year^{1}$ are located in the temperate forests and the lower NPP below 200 $gCm^{-2}year^{1}$ distributes in the cold or arid regions. But the simulated NPP of boreal forests is generally smaller than the IGBP data, especially in northern high latitudes. For instance, the simulation of Western Europe can be 200 $gCm^{-2}year^{1}$ lower in contrast to IGBP data. The reason is the cold bias of surface air temperature (Dan et al., 2005) due to less surface heating.

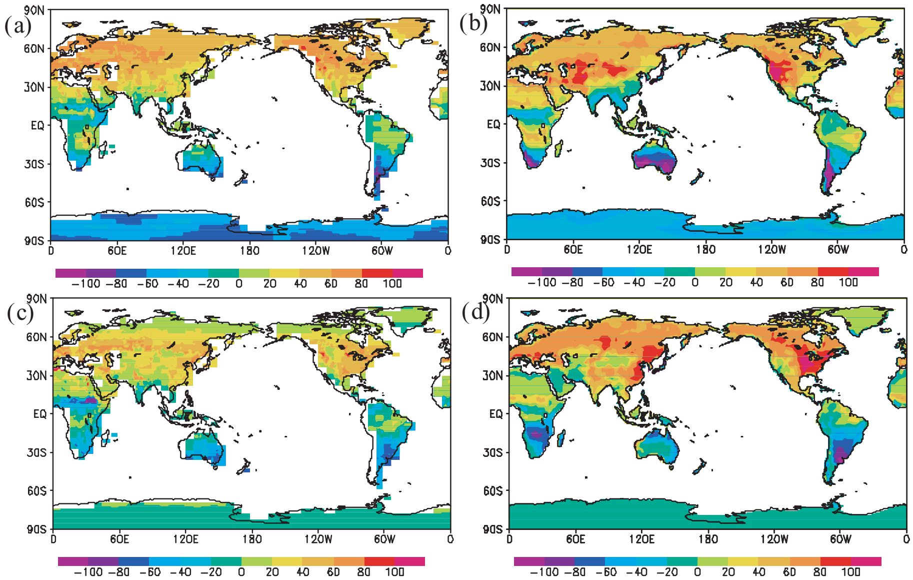

Fig. 2. As Fig. 1, but for the difference of July minus January sensible heat flux (SH) and latent heat flux (LH): (a) AVIM-GOALS SH difference, (b) ERA40 SH difference; (c) AVIM-GOALS LH difference, (d) ERA40 LH difference, units: Wm^{-2}.

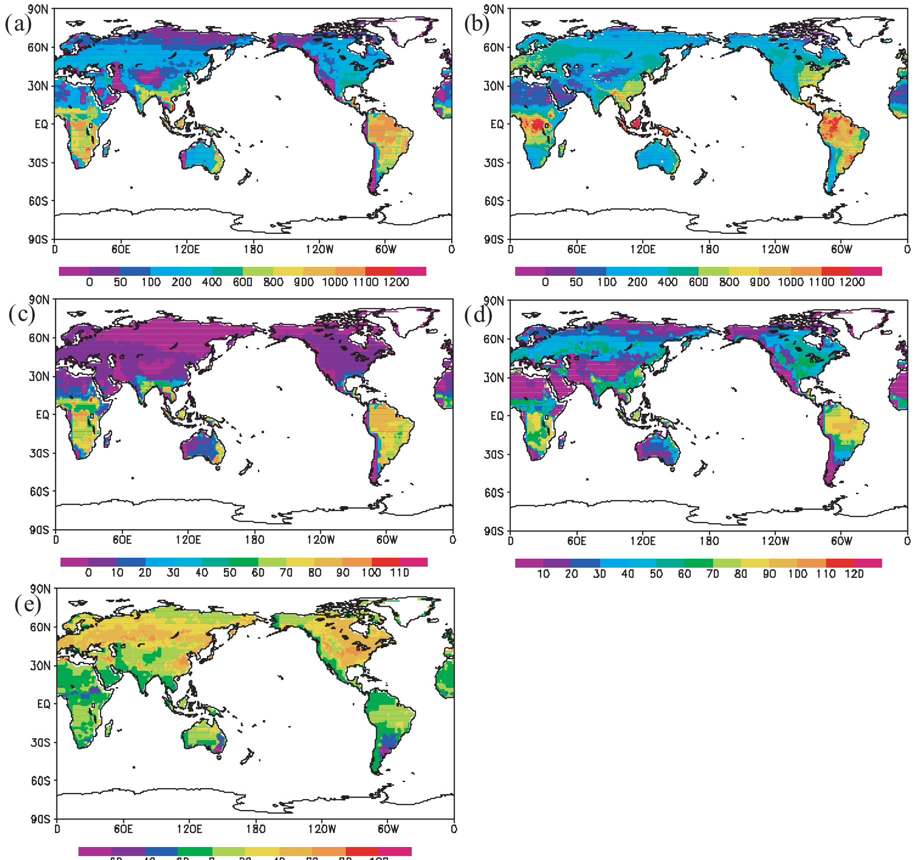

Fig. 3. The net primary production (NPP) for the coupled model AVIM-GOALS and IGBP model intercomparison average data: (a) Annual mean AVIM-GOALS NPP, (b) annual mean IGBP NPP, units: $gCm^{-2}year^{-1}$; (c) AVIM-GOALS NPP in January, (d) AVIM-GOALS NPP in July, (e) AVIM-GOALS NPP difference of July NPP minus January NPP, units: $gCm^{-2}month^{-1}$.

The simulation to south of 15 °S in Africa is larger than IGBP data mainly because of the land cover classification of broadleaf trees in contrast to grassland of other models (e.g. BIOME-BGC, Hunt et al., 1996).

In January, the simulated NPP (Fig. 3c) larger than 20 gCm^{-2}month^{-1} is mainly located to south of 30 °N, and a large area of the Northern Hemisphere is below 10 gCm^{-2}month^{-1}. The marked increase in July (Fig. 3d) occurs in the temperate and boreal forests in Northern Hemisphere, and the NPP of Southern Hemisphere shows the decrease to south of 15 °S. Fig. 3e is the difference between July and January NPP, and the major variation (>40 gCm^{-2}month^{-1}) is shown in the northern mid-latitudes (30–50 °N) as well as in southeast China and USA. Other regions vary little for NPP difference distribution, and the largest decrease below −20 gCm^{-2}month^{-1} occurs in Eastern Australia and southeastern South America.

(3) The LAI simulations

Due to the lack of global NPP observation and the IGBP model intercomparison. NPP data only available for annual average, the comparison of the simulated LAI against observation is one way to validate the simulated vegetation. NPP is closely related to the LAI through photosynthesis (see eq.(3) and (4)), and its variation can be reflected in the LAI change. Fig. 4a and b are the simulated and observed annual mean LAI, respectively. The global spatial pattern of LAI is similar to NPP distribution; in other words, the areas with large LAI generally have large NPP. The largest LAI (>8 m^{2}m^{-2}) is distributed throughout the tropical rainforests of Africa, Southeast Asia and Amozonia. The intermediate LAI (4–6 m^{2}m^{-2}) occurs in the temperate and boreal forests. The smallest LAI (<3 m^{2}m^{-2}) is located in the arid/semi-arid regions of the Sahara, Western China, Western coast of North America, and cold northern high latitudes. The seasonal variation magnitude of LAI is shown in Fig. 4c and d. The marked variation of the difference (>3 m^{2}m^{-2}) occurs in Northern Hemisphere including mid-latitudes, Eastern China and USA, But the simulated LAI variation amplitude in northern high latitudes is underestimated due to the lower July LAI affected by the cold bias of air temperature (Dan et al., 2005), which causes the lower NPP simulation. The seasonal variation of LAI in the arid regions and tropical rainforests is relatively small, reflecting the two extremes of LAI with a minimum for the former and a maximum for the latter, which indicates the stable state of vegetation in these regions. For the seasonal LAI difference of Southern Hemisphere, the positive difference emerges in Australia, but the largest value of the simulation is located in northern part in contrast to the southern part for observation, which can be attributed to the different spatial pattern of precipitation between the GCM simulation and observation (Dan et al., 2005). The vegetation of Australia is highly sensitive to precipitation changes (Barrett et al., 2002), thus the fact can be helpful to understand the discrepancy of LAI difference. The seasonal LAI difference in Southern Africa shows the reverse sign to observation due to the higher LAI in July resulting from the overestimated temperature and precipitation. The simulated seasonal LAI difference in South America is smaller in contrast to the observation, and this can be mainly attributed to the overestimated January LAI affected by a warm bias in simulated temperature in this region.

(4) The water use efficiency (WUE) simulations

The WUE is a variable that shows the plant dry matter per unit of water consumed and can be regarded as a link between the carbon cycle and the surface hydrological cycle. There are many

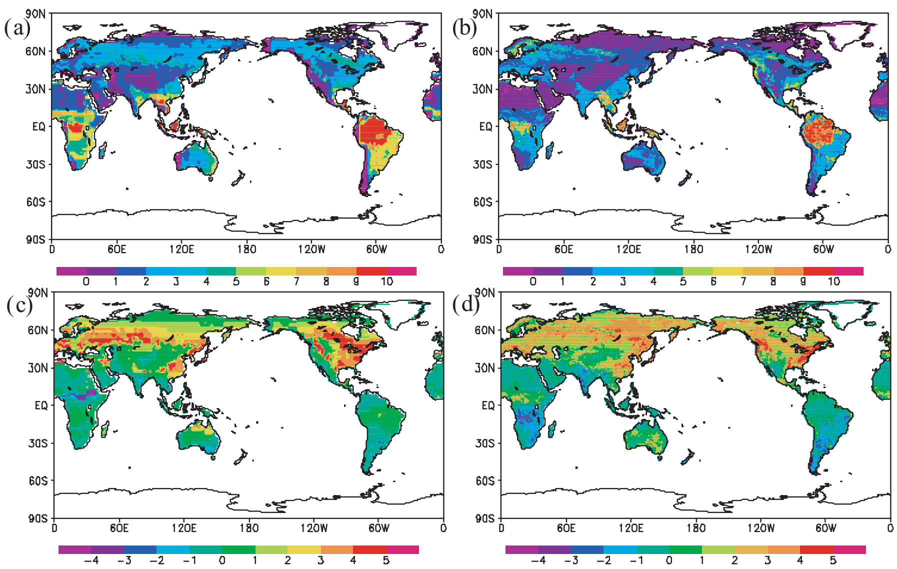

Fig. 4. (a) Annual mean leaf area index (LAI) of AVIM-GOALS, (b) annual mean observed LAI from Max Planck Institute for Meteorology; (c) AVIM-GOALS LAI difference of July LAI minus January LAI, (d) observed LAI difference of July LAI minus January LAI, units: m^{2}m^{-2}.

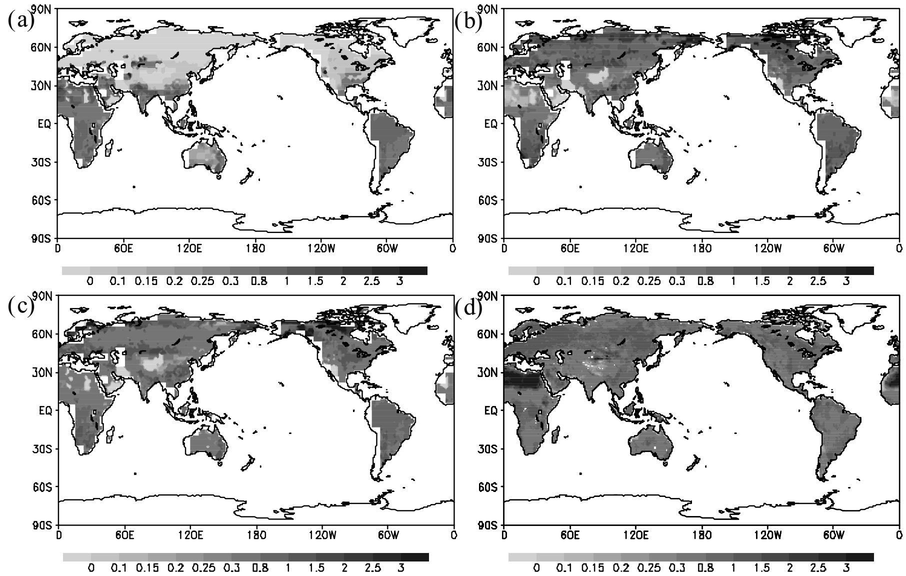

Fig. 5. The water use efficiency (WUE_T) defined as the ratio of NPP to evapotranspiration (ET): (a) AVIM-GOALS WUE_T in January, (b) AVIM-GOALS WUE_T in July; (c) AVIM-GOALS annual mean WUE_T, (d) reference WUE_T with the ratio of IGBP NPP to ERA40 ET, units: gkg^{-1}.

definitions of WUE, such as the WUE using transpiration at leaf scale and WUE using ET at canopy scale (Li et al., 2003 and Sun et al., 2006). In this study, WUE is defined as the ratio of NPP to the ET and is similar to definition of previous studies using the ratio of dry matter production to ET (Riedo et al., 1999). We use WUE_T to be distinguished from the WUE often using transpiration. Since the latent heat flux equals the total evaporation (including evaporation and transpiration), ET can be obtained from the LH by dividing the L of eq. (2). This index can show the NPP change with the energy variation related to the per unit water consumed. Fig. 5a and b present the global WUE_T simulation in January and July, respectively. The WUE_T in January is distributed mainly to south of 30 °N and the zero isoline reaches 50 °N of North America, which reflects the northern boundary of vegetation growth affected by the surface energy balance (with NPP > 0). In July, WUE_T presents the increase in the Northern Hemisphere and the value can be more than 1.0 gkg^{-1} in temperate forests, boreal forests and tundra. The seasonal variation of WUE_T in the Southern Hemisphere is smaller compared to the great change to north of 30 °N.

For the WUE_T comparison, the ratio of annual mean IGBP NPP to the ET transferred from annual ERA40 LH is used as the reference WUE_T and presented in Fig. 5d. The ERA40 ET is interpolated into 0.5 ° by 0.5 ° with the bilinear interpolation method. The reference WUE_T (Fig. 5d) and the simulated annual mean WUE_T (Fig. 5c) show the large value 1–1.5 gkg^{-1} in northern mid-latitudes, but the simulation in the boreal forests of Eurasia centered at 60 °N is lower than the reference WUE_T mainly due to the lower NPP. The simulated WUE_T is much lower than the reference WUE_T in Sahara and the maximum reference WUE_T in Sahara can be attributed to the quite small ERA40 LH of desert (most energy partitioning into SH). The reason of the smaller simulated WUE_T in this region is that the vegetation type of the coupled model is the broadleaf shrubs with bare soil (Dan et al., 2005) of which the simulated LH is higher than that of desert in ERA40 data (cf. Fig. 1c and d). The simulated annual WUE_T in northern high latitudes, especially in North America, seems to be overestimated due to the lower simulated LH. The reason is a smaller heat surplus from the radiation budget, which induces the small LH in this region.

3.2. *The seasonality of SPFs, NPP and LAI*

The vegetation phenology exists across the globe: vegetation growth in summer and dormancy (falling leaf) in winter. For the global vegetation, what is seasonal cycle distribution, and what region shows the most drastic seasonality? To study the global seasonality of physical fluxes and vegetation, the monthly time series of global mean SPFs, LAI and NPP were calculated by the transfer of opposite season in Southern Hemisphere (according to the onset and offset month of four seasons in Northern Hemisphere) to obtain the uniform season shift across the globe. The correlation coefficient between the monthly mean variable and its globally averaged value is shown in Fig. 6 and Fig. 7. The seasonal adjustment of the Southern Hemisphere according to the vegetation onset and offset time of the Northern Hemisphere does not affect the basic pattern of the global significance level. Without the adjustment, only present positive correlation in the regions south of 15 °S in Fig. 6 and Fig. 7 will be negative coefficients (Figures not shown). This accounts for the fact that seasonal cycle at land areas of the Southern Hemisphere is less significant than that of the Northern Hemisphere, and the major contributor to the global seasonality is located in the Northern Hemisphere.

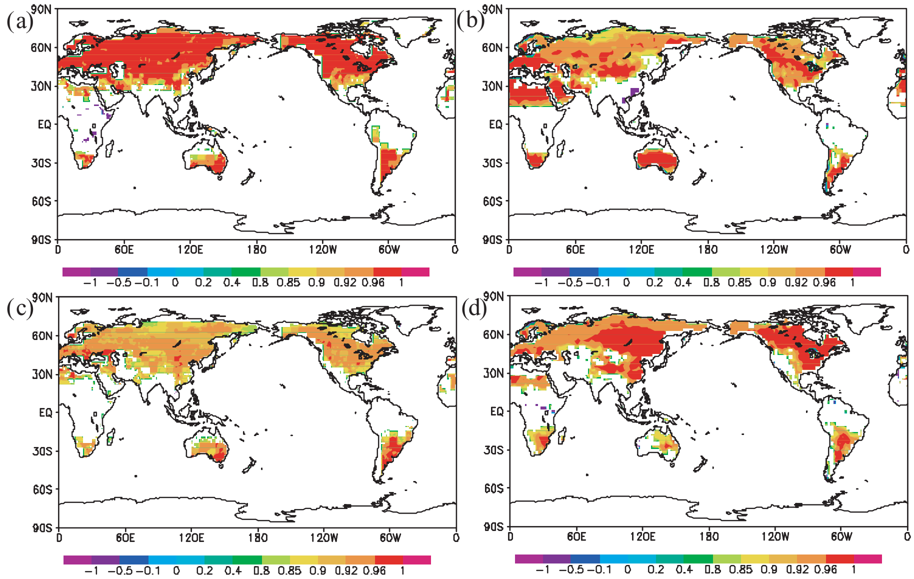

Fig. 6. The correlation coefficients between the monthly mean variable and its globally averaged monthly mean value: (a) For AVIM-GOALS sensible heat flux (SH), (b) for ERA40 SH; (c) For AVIM-GOALS latent heat flux (LH), (d) for ERA40 LH. (seasonal adjustment over Southern Hemisphere according to the onset and offset time of Northern Hemisphere, only values above 99.9% significance level presented)

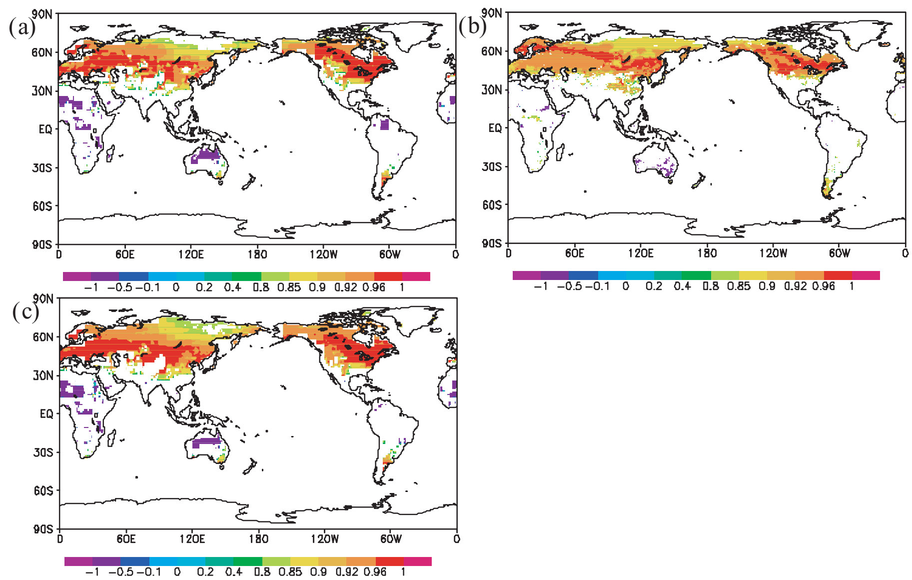

Fig. 7. As Fig. 6, but for leaf area index and NPP: (a) AVIM-GOALS LAI correlation coefficient, (b) observed LAI correlation coefficient (data from Max Planck Institute for Meteorology); (c) AVIM-GOALS NPP correlation coefficient. (seasonal adjustment over Southern Hemisphere according to the onset and offset time of Northern Hemisphere, only values above 99.9% significance level presented)

The seasonal cycle of SPFs plays an important role in climate change. For example, the seasonal heating of SH can be helpful to simulate the abrupt northward jump of the eastern Asian monsoon (Xue et al., 2004). Fig. 6 shows the global terrestrial correlation coefficients of SH and LH with their global monthly mean values over land. The areas with statistical significance of 99.9% using the Student's t-test are mainly located to north of 30 °N and south of 15 °S. But due to the relatively small area of Southern Hemisphere passing the significance level in contrast to that of Northern Hemisphere, only the seasonality in Northern Hemisphere is analyzed in this study. The seasonality in low latitudes is so weak with a lower significance and the correlation has large spatial heterogeneity (the positive and negative correlation coexists in this region). The correlation coefficient of LH in northern mid-latitudes shows the largest value above 0.94. What should be noticed is the global monthly means averaged over land areas, and this kind of correlation excludes the impact of oceans.

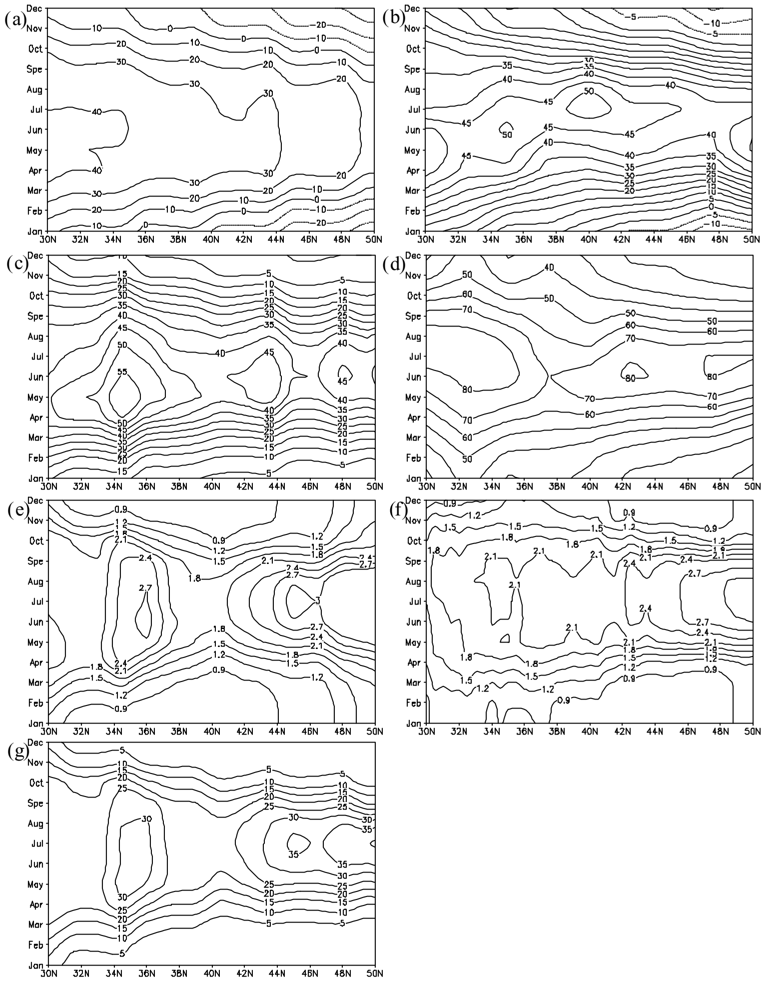

Fig. 8. The 30 °N–50 °N zonal mean of monthly mean fluxes and LAI: (a) AVIM-GOALS sensible heat flux (SH), (b) ERA40 SH; (c) AVIM-GOALS latent heat flux (LH), (d) ERA40 LH, units: Wm^{-2}. (e) The simulated leaf area index (LAI) of AVIM-GOALS, (f) the observed LAI, units: m^2/m^2. (g) The simulated NPP of AVIM-GOALS, units: $gCm^{-2}month^{-1}$.

The correlation coefficients for LAI and NPP with their corresponding global averages are shown in Fig. 7. The correlation coefficients distribution is similar to that of SH and LH. However, most regions in Africa and northern high latitudes of Eurasia cannot pass the significance test, especially for LAI. The correlation coefficient of simulated LAI (Fig. 7a) agrees well with that of the observation (Fig. 7b), presenting large value above 0.92 in northern mid-latitudes, where the biggest contributor to global seasonality exists. Consequently, the 30 °N–50 °N region was chosen to analyze the seasonality of SPFs, LAI and NPP.

The zonal mean of SPFs, LAI and NPP between 30 °N–50 °N in each month is shown in Fig. 8. All variables in this statistical sensitive region present the marked seasonal variation, high in summer and low in winter. There are three peaks around 34 °N, 42 °N and 48 °N in the month-latitude variation of SPFs, LAI and NPP. The nearly simultaneous variation of SPFs and vegetation along latitude in this region is the indication of the close linkage between them. It is due to the interaction of the energy and water cycle that the SPFs and vegetation show the inter-correlated seasonality in the coupled model. The simulated LAI variation (Fig. 8e) is corresponding to the observation (Fig. 8f), which shows the LAI above 1.8 m^2m^{-2} from April to September and below 1.2 m^2m^{-2} in boreal winter. The noticeable seasonality also exists for NPP, above 30 $gCm^{-2}month^{-1}$ in summer and below 10 $gCm^{-2}month^{-1}$ in winter. This phenomenon may explain the large amplitude of seasonal cycle of surface CO_2 in Northern Hemisphere mid-latitudes (Olsen et al., 2004). The simulated magnitude of SPFs is generally lower than the ERA40 data, especially for the LH, and the maximum discrepancy can reach 35 Wm^{-2}.

To test the degree of correlation of the SH, LH, LAI and NPP in northern mid-latitudes, the correlation coefficients of any area-averaged variable in each month in this 30 °N–50 °N region with others are presented in Table 3. All the correlation coefficients in the Table 3 show the high statistical significance and nearly pass the 99.9% level (only one coefficient between the observation LAI and modelled SH passing 99.5%) in the Student's t-test. The high correlation with high significance presents the close linkage of the seasonality in northern mid-latitudes for surface

Table 3. The correlation coefficients between any modelled and observed variable among area-averaged monthly mean sensible heat flux (SH), latent heat flux (LH), LAI and NPP for terrestrial 30 °N–50 °N. The symbol 'M' means 'simulation', 'O' for 'observation' and 'R' for reanalysis data

Correlation coefficient	SH_M (Wm^{-2})	LH_M (Wm^{-2})	LAI_M (m^2m^{-2})	NPP_M ($gCm^{-2}month^{-1}$)
SH_R	0.985	0.995	0.943	0.954
LH_R	0.927	0.978	0.985	0.988
LAI_O	0.819*	0.866	0.978	0.977
Remark	The number with asterisk means passing 99.5% significance level, others for 99.9% level.			

energy, water and carbon flux, which shows the most marked seasonality in this region across the globe.

4. Discussion

The SPFs, LAI and NPP are key variables to represent the energy and water exchange, vegetation morphology variation and carbon exchange at the land/air interface. The SPFs are regarded as the physical processes (Lu and Ji, 2002a), and vegetation processes including structure and functioning belong to ecological field. However, the physical and ecological variation should be linked in mechanism to study their interaction. To study the feedbacks between physical climate system and vegetation, the coupled ocean-atmosphere-carbon model is a good choice (Govindasamy et al., 2005) This kind of linkage has been realized in the two-way coupled model AVIM-GOALS, which helps to study the interaction of surface energy, water flux and terrestrial carbon cycle. This study analyzed the global pattern and the magnitude of SPFs, LAI and NPP, and explored the relationship between physical fluxes and biological fields in global seasonality.

Although to accurately quantify the global SPFs is difficult, the intercomparison of modelled SPFs to reanalysis is one method to understand strength and weakness of representation of SPFs in LSMs. Previous studies have analyzed SPFs over oceans, such as Yu and Mechoso (1999) analyzed the modelled LH errors in the tropical Pacific Ocean. Frankignoul et al. (2004) compared modelled SPFs over global ocean to NCEP reanalysis and found the strong SPFs feedback effect at the extratropical ocean. In this paper, we analyzed the global terrestrial SPFs and found the strong signal in its seasonality located in northern mid-latitudes. The simulated SPFs distribution corresponds to ERA40 flux data across the globe. The discrepancy of SPFs is the overall lower value in contrast to ERA40 flux derived from the data assimilation model, such as the 20 Wm^{-2} lower in northern high latitudes. The shortage of radiation surplus in northern high latitudes can account for the lower simulated SPFs. However, the SPFs difference in magnitude can be understood since different LSMs adopt different parametrization for SPFs, similar to the discrepancy of LSMs driven by the same meteorological conditions of PILPS (Pitman et al., 1999). The seasonal oscillation amplitude, represented by the July SPFs minus the January SPFs, is consistent with ERA40 data. The absolute value of SH in seasonal change (above 40 Wm^{-2}) emerges in extratropical land areas north of 30 °N and south of 30 °S. The seasonal difference of LH shows a large positive value up to 80 Wm^{-2} in boreal forests, but the simulation is 20 Wm^{-2} smaller than the ERA40 LH difference, even up to 40 wm^{-2} in Eastern China and USA.

The simulations show that the spatial pattern of annual NPP agree with IGBP NPP data from 0–200 $gCm^{-2}year^{-1}$ in arid and cold regions to high value above 1000 $gCm^{-2}year^{-1}$ in tropical rainforests. The simulated NPP in northern high latitudes is underestimated due to the lower simulated temperature and the value south of 15 °S is overestimated because of the land cover types used here different from other vegetation models. Due to the opposite season in contrast to Northern Hemisphere, the NPP difference between January and July shows the decrease in Southern Hemisphere with the negative centre in Eastern Australia and southeastern South America. The simulated annual mean LAI corresponds to the observation: above 8 m^2m^{-2} for rainforests and 4–6 m^2m^{-2} for temperate forests and boreal forests. The simulated seasonal difference in LAI above 2 m^2m^{-2} is mainly located in Eastern China, Eastern USA and boreal forests, which agrees with the observation magnitude of July–January difference in these regions.

As a variable linking carbon with water flux, the water use efficiency shows a large seasonal increase in extratropical regions over land, especially in northern mid to high latitudes. The annual mean WUE_T of the coupled model is roughly consistent with the reference WUE_T. Compared to WUE using transpiration in the calculation, WUE_T incorporating evaporation from the soil has the large difference in transitional regions (semi-arid regions, e.g. northwestern China and southeastern USA), where the soil evaporation can be comparable to vegetation transpiration due to the comparatively adequate amounts of soil water and surface energy. In these transitional regions, WUE_T is lower than WUE because soil evaporation can be up to 40–80% of ET. In forest regions, the effect of soil evaporation on WUE_T can be neglected in regards to WUE. Transpiration in forests dominates the calculation of WUE_T or WUE because the magnitude of soil evaporation is much smaller than vegetation transpiration. In the desert, the values of NPP, soil evaporation and ET are small, thus it is hard to evaluate the difference between WUE_T and WUE, and the equations of soil transpiration and ET can be found in the appendix A2 of Lu and Ji (2006).

To investigate the seasonality of SPFs and vegetation, the region with high statistical significance (99.9%) was found by calculating the correlation coefficient between the variable and its global monthly average. The seasonal cycle of SPFs is important to climate predictability, and is most pronounced over mid-latitude continental regions and less so over the oceans and at lower latitudes (Elsner et al., 1994). The reason for the enhanced predictability in northern mid-latitudes is the dependence of tropospheric heating related to SH (Elsner et al., 1994), thus the northern mid-latitudes are unique for climate study. For the carbon cycle, land-use change has strong impact on the carbon storage in this region (Zhuang et al., 2003) and the northern mid-latitudes including Eurasian boreal and North American temperate forests have been large variable carbon sink since 1981 (Barford et al., 2001; Myneni et al., 2001; Cao et al., 2005). Consequently, the northern mid-latitudes are key regions to study the interaction between SPFs and terrestrial carbon. The largest contributor to the global seasonal variation is the northern mid-latitudes with correlation coefficient above 0.92. The correlation can not be altered by the opposite season phase of the Southern Hemisphere compared with the Northern Hemisphere, which shows the strong seasonality in contrast to SH, LH, LAI and NPP of other regions across the globe. The interaction between the physical fluxes and vegetation can be reflected in the zonal mean fields as well as the correlation coefficients for any two area-averaged variables. The month-latitude distribution between 30 °N–50 °N shows the three-peak seasonal variation for SPFs, LAI and NPP. The obvious discrepancy is the lower simulated LH in contrast to ERA40 LH data. The correlation coefficients between any two fields present high statistical significance: one for the 99.5% level and eleven for the 99.9%.

5. Conclusions

We have coupled the new version of AVIM into GOALS GCM and explored the global surface water, energy and carbon flux in the two-way coupled model. The SPFs are related to the terrestrial ecosystem through the energy and water budget at the surface as well as the morphology of vegetation (e.g. LAI). Our results show that the SPFs, LAI and NPP are generally consistent with ERA40 reanalysis, observation LAI and IGBP model intercomparison NPP, respectively, in the global spatial pattern and seasonal oscillation amplitude. Our results also indicate that the main contributor to global mean seasonality of surface fluxes over land is located in northern mid-latitudes, and the strong contribution can not be changed by the opposite season of Southern Hemisphere in contrast to Northern Hemisphere. The seasonality contribution has high statistical significance of 99.9% confidence level in the Student's t-test, and the significant seasonality occurs in the region of 30–50 °N for the SPFs, LAI and NPP.

6. Acknowledgments

This work was supported by the Innovation Project of Chinese Academy of Sciences (grant No. KZCX3-SW-229), the State Key Basic Development Planning Project (grant no. 2006CB400506 and G2002CB412500) and project of National Natural Science Foundation of China (grant no.40605025). We'd like to thank Mr. Christopher Michael Brodowski, Dr. J.H. Lu, Dr. Y.P. Li and his colleagues for the language editing of this paper.

References

Barford, C. C., Wofsy, S. C., Goulden, M. L., Munger, J. W., Pyle, E. H. and co-authors 2001. Factors controlling long- and short-term sequestration of atmospheric CO_2 in a mid-latitude forest. *Science* **294**, 1688–1691.

Barrett, D. J. 2002. Steady state turnover time of carbon in the Australian terrestrial biosphere. *Global Biogeochem. Cycles* **16**, 1108, doi:10.1029/2002GB001860.

Cao, M. K., Prince, S. D., Tao, B., Small, J. and Li, K. R. 2005. Regional pattern and interannual variations in global terrestrial carbon uptake in response to changes in climate and atmospheric CO_2. *Tellus* **57B**, 210–217.

Chen, F. and Dudhia, J. 2001. Coupling an advanced land surface–hydrology model with the Penn State–NCAR MM5 modeling system Part I: model implementation and sensitivity. *Mon. Weather Rev.* **129**, 569–585.

Chen, T. H., Henderson-sellers, A., Milly, P. C. D. and co-authors. 1997. Cabauw experimental results from the Project for Intercomparison of Land-Surface Parametrization Schemes. *J. Clim.* **10**, 1194–1215.

Collatz, G., Ribas-Carbo, M. and Ball, J. A. 1992. Coupled photosynthesis-stomatal conductance model for leaves of C4 plants. *Australian J. Plant Physiol.* **19**, 519–538.

Cox, P. M., Betts, R. A., Jones, C. D., Spall, S. A. and Totterdell, I. J. 2000. Acceleration of global warming due to carbon-cycle feedbacks in a coupled climate model. *Nature* **408**, 184–187.

Coquard, J., Buffy, P. B., Taylor, K. E. and Iorio, J. P. 2004. Present and future surface climate in the western USA as simulated by 15 global climate models. *Clim. Dyn.* **23**, 455–472.

Cramer, W., Kicklighter, D. W., Bondeau, A., Moore, B., Churkina, G. and co-authors and the participants of the Potsdam NPP Model Intercomparison. 1999. Comparing global models of terrestrial net primary productivity (NPP): overview and key results. *Global Change Biol.* **5**(**Suppl. 1**), 1–15.

Dan, L., Ji, J. J. and Li, Y. P. 2005. Climatic and biological simulations in a two-way coupled atmosphere-biosphere model (CABM). *Glob. Planet. Change* **47**, 153–169.

Elsner, J. B. and Tsonis, A. L. A. 1994. Empirically derived climate predictability over the extratropical northern hemisphere. *Nonlinear Process. Geophys.* **1**, 41–44.

Farquhar, G. D., Caemmerer, S. von and Berry, J. A. 1980. A biochemical model of photosynthetic CO2 assimilation in leaves of C3 plants. *Planta* **149**, 78–90.

Farquhar, G. D. and Sharley, T. D. 1982. Stomatal conductance and photosynthesis. *Annu. Rev. Plant Physiol.* **33**, 317–345.

Field, C. B. 1983. Allocating leaf nitrogen for the maximization of carbon gain: Leaf age as a control on the allocation program. *Oecologia* **56**, 341–347.

Frankignoul, C., Kestenare, E., Botzet, M., Carril, A. F., Drange, H. and co-authors. 2004. An intercomparison between the surface heat flux feedback in five coupled models, COADS and the NCEP reanalysis. *Clim. Dyn.* **22**, 373–388.

Friedlingstein, P., Bopp, L., Ciais, P., Dufresne, J., Fairhead, L. and co-authors. 2001. Positive feedback between future climate change and the carbon cycle. *Geophys. Res. Lett.*, **28**, 1543–1546.

Gao, G. D. and Lu, Y. R. 1981. *Climatological atlas of China*. China Agriculture Publishing House, 1–183 (in Chinese).

Govindasamy, B., Thompson, S., Mirin, A., Wickett, M., Caldeira, K. and co-authors. 2005. Increase of carbon cycle feedback with climate sensitivity: results from a coupled climate and carbon cycle model. *Tellus* **57B**, 153–163.

Hagemann, S., Botzet, M., Dumenil, L. and Machenhauer, B. 1999. *Derivation of global GCM boundary conditions from 1 KM land use satellite data*. Max Planck Institute for Meteorology (MPI) Report No. 289, 1–34.

Hagemann, S. 2002. *An improved land surface parameter dataset for global and regional climate models*. Max Planck Institute for Meteorology (MPI) Report No.336, 1–21.

Hunt, E. R., Piper, S. C., Nemani, R., Keeling, C. D., Otto, R. D. and co-authors. 1996. Global net carbon exchange and intra-annual atmospheric CO_2 concentrations predicted by an ecosystem process model and three-dimensional atmospheric transport model. *Global Biogeochem. Cycles* **10**, 431–456.

Imhoff, M. L., Bounoua, L., Ricketts, T., Loucks, C., Harriss, R. and co-authors. 2004. Global patterns in human consumption of net primary production. *Nature* **429**, 870–873.

Jacobs, C. M. J., van den Hurk, B. J. J. M. and de Bruin, H. A. R. 1996. Stomatal behaviour and photosynthetic rate of unstressed grapevines in semi-arid conditions. *Agric. Forest Meteorol.* **80**, 111–134.

Ji, J. J. 1995. A climate-vegetation interaction model: simulating physical and biological processes at the surface. *J. Biogeogr.* **22**, 445–451.

Ji, J. J., and Hu, Y. C. 1989. A simple land surface process model for use in climate studies. *Acta Meteorol. Sinica* **3**, 344–353.

Ji, J. J. and Yu, L. 1999. A simulation study of coupled feedback mechanism between physical and biogeochemical processes at the surface. *Chinese J Atmos. Sci.* **23**, 439–448 (in Chinese).

Ji, J. J., Huang, M. and Liu, Q. 2005. Modeling studies of response mechanism of steppe productivity to climate change in middle latitude semiarid regions in China. *Acta Meteorol. Sinica* **63**, 257–266 (in Chinese).

Koster, R. D., Dirmeyer, P. A., Hahmann, A. N., Ijpelaar, R., Tyahla, L. and co-authors. 2002. Comparing the degree of land–atmosphere interaction in four atmospheric general circulation models. *J. Hydrometeorol.* **3**, 363–375.

Li, F. S., Kang, S. Z. and Zhang, F. C. 2003. Effects of CO_2 enrichment, nitrogen and water on photosynthesis, evapotranspiration and water use efficiency. *Chinese J.f Applied Ecol.* **14**, 387–393 (in Chinese).

Li, Y. P. and Ji, J. J. 2001. Model estimates of global carbon flux between vegetation and the atmosphere. *Advance Atmos. Sci.* **18**, 807–818.

Liu, Y. M., Wu, G. X., Liu, H. and Liu, P. 2001. Condensation heating of the Asian summer monsoon and the subtropical anticyclone in the Eastern Hemisphere. *Clim. Dyn.* **19**, 327–338.

Liu, Y. M., Wu, G. X. and Ren, R. C. 2004. Relationship between the subtropical anticyclone and diabatic heating. *J. Clim.* **17**, 682–698.

Lu, J. H. and Ji, J. J. 2002a. A simulation study of atmosphere-vegetation interactions over the Tibetan Plateau, Part I: physical flux and parameters. *Chinese J. Atmos. Sci.* **26**, 111–126 (in Chinese).

Lu, J. H. and Ji, J. J. 2002b. A simulation study of atmosphere-vegetation interactions over the Tibetan Plateau, Part II: net primary productivity and leaf area index. *Chinese J. Atmos. Sci.* **26**, 254–262 (in Chinese).

Lu, J. H. and Ji, J. J. 2006. A simulation and mechanism of long-term variations at land surface over arid/semi-arid area in north China. *J. Geophys. Res.* **111**, D09306, doi:10.1029/2005JD006252.

Myneni, R. B. Dong, J., Tucker, C. J., Kaufmann, R. K., Kauppi, P. E. and co-authors. 2001. A large carbon sink in the woody biomass of northern forest. *Proc. Natl. Acad. Sci.* **98**, 4784–14789.

Olsen, S. C. and Randerson, J. T. 2004. Differences between surface and column atmospheric CO2 and implications for carbon cycle research. *J. Geophys. Res.* **109**, D02301, doi:10.1029/2003JD003968.

Phillips, N. A. 1973. Principles of large scale numerical weather prediction. In: *Dynamic Meteorology* (ed. P. Morel). D. Reidel Publishing Comp, Dordrecht, Holland, pp 96.

Pitman, A. J., Henderson-seller, A., Desborough, C. E., Yang, Z. L., Abramopoulos, F. and other co-authos. 1999. Key results and implications from phase1(c) of the Project for Intercomparison of Land-surface Parametrization Schemes. *Clim. Dyn.* **15**, 673–684.

Riedo, M., Gyalistras, D., Fischlin, A. and Fuhrer, J. 1999. Using an ecosystem model linked to GCM-derived local weather scenarios to analyse effects of climate change ande levated CO2 on dry matter production and partitioning, and water use in temperate managed grasslands. *Global Change Biol.* **5**, 213–223.

Schulze, E. D., Kelliher, F. M., Ko¨rner, C., Lloyd, J. and Leuning, R. 1994. Relationships among maximum stomatal conductance, ecosystem surface conductance, carbon assimilation rate, and plant nitrogen nutrition: A global ecology scaling exercise. *Annual Rev. Ecol. Systematics* **25**, 629–660.

Sellers, P. J., Dickinson, R. E., Randall, D. A., Betts, A. K., Hall, F. G. and co-authors. 1997. Modelling the exchanges of energy, water and carbon between the continents and the atmosphere. *Science* **275**, 502–509.

Shao, Y. and Henderson-Sellers, A. 1996. Modeling soil moisture: a Project for Intercomparison of Land Surface Parametrization Schemes Phase2 (b). *J. Geophys. Res.* **101**, 7227–7250.

Shukla, J. and Mintz, Y. 1982. Influence of land-surface evapotranspiration on the earth's climate. *Science* **215**, 1498–1501.

Simmons, A. J. and Gibson, J. K. 2000. *The ERA-40 project plan*. ERA-40 Project Report Series 1, ECMWF, Shinfield Park, Reading, United Kingdom, pp. 63.

Sun, H. Y., Liu, C. M., Zhang, X. Y., Shen, Y. J. and Zhang, Y. Q. 2006. Effects of irrigation on water balance, yield and WUE of winter wheat in the North China Plain. *Agric. Water Manage.* **85**, 211–218.

Varejao-Silva, M. A., Franchito, S. H. and Rao, V. B. 1998. A coupled biosphere–atmosphere climate model suitable for studies of climatic change due to land surface alterations. *J. Clim.* **11**, 1749–1767.

Wang, B., Liu, H. and Shi, G. Y. 2000. In: *Chapter 3: Radiation and cloud scheme, IAP Global Ocean Atmosphere-Land System Model* (eds. X. H. Zhang et al.). Science Press, Beijing, New York, pp. 28–49.

Woodward, F. I., Smith, T. M. and Emanuel, W. R. 1995. A global land primary productivity and phytogeography model. *Global Biogeochem. Cycles* **9**, 471–490.

Wu, G. X., Zhang, X. H., Liu, H., Yu, Y. Q., Jin, X. Z. and co-authors. 1997. Global ocean-atmosphere-land system model of LASG (GOALS/LASG) and its performance in simulation study. *Q.J. Appl Meteorol.* **8**, 15–28 (in Chinese).

Xue, Y., Juang, H. M. H., Li, W. P., Prince, S., DeFries, R. and co-authors. 2004. Role of land surface processes in monsoon development: East Asia and West Africa *J. Geophy. Res.* **109**, D03105, doi:10.1029/2003JD003556.

Yu, J. Y. and Mechoso, C. R. 1999. A discussion on the errors in the surface heat fluxes simulated by a coupled GCM. *J. Clim.* **12**, 416–426.

Zeng, Q. C. 1963. Characteristic parameters and dynamical equations of atmospheric motions. *Acta Meteorol. Sinica*, **33**, 472–498 (in Chinese).

Zhang, T., Wu, G. X. and Guo, Y. F. 2002. Energy budget bias in global coupled ocean-atmosphere-land model. *Acta Meteorol. Sinica* **60**, 278–289 (in Chinese).

Zheng, D. L., Prince, S. and Wright, R. 2003. Terrestrial net primary production estimates for 0.5o grid cells from field observations- a contribution to global biogeochemical modelling. *Global Change Biol.* **9**, 46–64.

Zhuang, Q., Mguire, A. D., Melillo, J. M., Clein, J. S., Dargaville, R. J. and co-authors. 2003. Carbon cycling in extratropical terrestrial ecosystems of the Northern Hemisphere during the 20th century: a modeling analysis of the influences of soil thermal dynamics. *Tellus* **55B**, 751–776.

Zobler, L. 1986. *A world soil file for global climate modeling*. NASA Tech. Memo. 87802, NASA Goddard Institute for Space Studies, New York, USA, 1–33.